Multiple Substrate Binding States and Chiral Recognition in Cofactor-independent Glutamate Racemase: A Molecular Dynamics Study†

Henrik Möbitz and Thomas C. Bruice*

Department of Chemistry and Biochemistry, University of California, Santa Barbara, Santa Barbara, California 93106

Received March 1, 2004; Revised Manuscript Received April 15, 2004

ABSTRACT: Glutamate racemase (MurI) catalyzes the racemization of glutamate; two cysteine residues serve as catalytic acid and base. On the basis of the crystal structure of MurI from the hyperthermophilic bacterium *Aquifex pyrophilus*, we performed molecular dynamics (MD) simulations of six different systems to investigate stereochemistry, substrate ligation, and active site protonation state. The catalytic competence of individual systems was assessed by the abundance of reactive conformers. Only systems in which Cys70 is poised to deprotonate D-Glu were found to be catalytically competent (idem Cys178/L-Glu), in agreement with the experimentally observed stereochemistry of *Lactobacillus fermentii* MurI [Tanner, M. E. et al. (1993) *Biochemistry 32*, 3998−4006]. Only systems in which the α-amino group of L/D-Glu and the imidazole moiety of His are deprotonated are catalytically competent. The active site of MurI displays an unusual flexibility in substrate ligation, and several transitions between stable binding patterns were observed. In catalytically competent binding states, the conserved threonine residues 72, 114, and 117 ligate the α-carboxylate of Glu and the Asn71 amides ligate the α-amino group of Glu, whereas the δ-carboxylate of Glu is steered by electrostatic repulsion from the Asp7 and Glu147 side chain carboxylates. A network of hydrogen bonds controls the positioning of each thiol/thiolate. In what we term substrate flipping, Glu suddenly rotates into a binding pattern that resembles the post-racemization state of the other enantiomer, i.e., each enantiomer can be bound in two distinct states. Substrate flipping and unfavorable substrate binding successively trigger dissociation of the substrate, accompanied by an opening of the active site channel. We explain how the weak binding of Glu contributes to catalysis and suggest a mechanism by which binding mismatches are propagated into an opening of the active site.

In many forms of life, D-amino acids play important, highly specific roles, e.g., as building blocks in the bacterial cell wall or as neurotransmitters in mammals. They are synthesized from L-amino acids by amino acid racemases (AAR).[1] While most AARs employ the cofactor pyridoxalphosphate (PLP) to achieve the difficult abstraction of the Hα proton, another group of AARs has fascinated biochemists by its absence of cofactors and metal ions. This group includes glutamate racemase (MurI, *1*), aspartate racemase (AspR, *2*), diaminopimelate epimerase (*3*), and proline racemase (*4*). In pioneering work on proline racemase, the groups of Knowles and Abeles established that two cysteine residues function as catalytic acid and bases (*5*), with one cysteine thiolate attacking Hα to form an enolate anion and the other cysteine thiol donating a proton from the opposite side, thus achieving racemization (Scheme 1, *6*). Abstraction of Hα is rate-limiting, and protonation of the enolate species is supposed to occur immediately ($k_{+H} \sim 10^{12}$ s^{-1}). The active site exists in two protonation states that are responsible for the binding and interconversion of only one enantiomer (*4*, *5*).

Scheme 1: Paradigm for the Catalytic Cycle of PLP-Independent Amino Acid Racemases, Derived from Kinetic Studies on Proline Racemase[a]

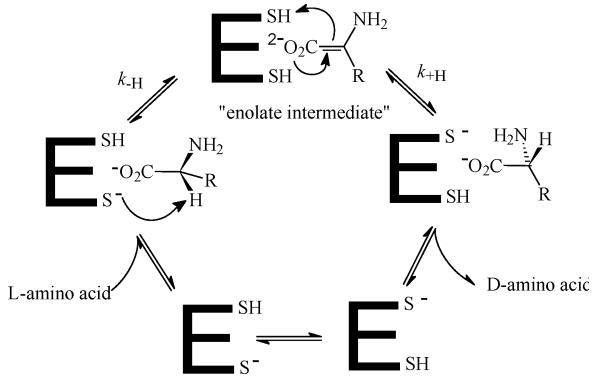

[a] Ref *6*.

The principal findings on the mechanism of proline racemase were also found to be valid for glutamate racemase, MurI. To this date, the enzyme from *Lactobacillus fermentii* remains the best studied example of MurI (*1*, *7*−*10*). Abstraction of Hα was found to be (partially) rate limiting and mutation of either conserved cysteine into alanine abolishes racemase activity but results in proteins that are still able to stereospecifically remove a proton from opposite

† This work was supported by Grants MO 1070/1-1 from the Deutsche Forschungsgesellschaft to H.M. and the National Science Foundation (Grant MCB-0129568) to T.C.B.

* To whom correspondence should be addressed: Thomas C. Bruice. Phone: (805) 893-2044. Fax: (805) 893-2229. E-mail: tcbruice@chem.ucsb.edu.

[1] Abbreviations: AAR, amino acid racemase; AspR, aspartate racemase; MD, molecular dynamics; MurI, glutamate racemase; PLP, pyridoxalphosphate; RMSD, root-mean-square deviation.

10.1021/bi049580t CCC: $27.50
Published on Web 07/10/2004

Table 1: Summary of Setups

	AD3	AL2	AL3	HIS	GLU	298
Cys70 poised to deprotonate	L-Glu	D-Glu	D-Glu	D-Glu	D-Glu	D-Glu
Cys178 poised to deprotonate	D-Glu	L-Glu	L-Glu	L-Glu	L-Glu	L-Glu
Glu α-NH_3^+ group	−	−	−	−	+	−
His180 protonated	−	−	−	+	−	−
initial restraints on S···Hα	−	−	+	+	+	+
constrained surface lysines	+	+	+	+	+	−
simulation temperature [K]	358	358	358	358	358	298
total simulation time [ps]	1800	2100	2100	1250	1440	1250
time required for eqn. [ps]	300	190	300	300	300	300
RMSD [Å]	1.3 ± 0.1	1.0 ± 0.2	1.4 ± 0.2	1.1 ± 0.1	1.1 ± 0.1	1.1 ± 0.3
RMSD drift 0.3−2 ns [Å/ns]	0.2/0.1	0.03/0.1	0.2/0.2	0.1/0.3	0.2/0.1	0.08/0.01

enantiomers of *threo*-3-chloroglutamate (*8*). This finding and matching asymmetric kinetic isotope effects of the Cys73Ser and Cys184Ser mutants showed that Cys73 is responsible for the deprotonation of D-glutamate, while Cys184 deprotonates the L-enantiomer (*9*). Mutation of conserved Glu, Asp, and His residues clustered around conserved motifs resulted in significant effects on k_{cat} or K_m (*10*). This observation suggested that these residues are involved in the protonation network around the catalytic residues. The crystal structure of *Aquifex pyrophilus* glutamate racemase confirmed that several of these residues are indeed located in the active site.

A. pyrophilus MurI is a homodimer of 254 amino acid residues, whose subunits are made up by two compact domains with α/*β*-structure (*11*). The active site is located between these domains with the Glu147 loop of the second subunit participating in it (noted Glu′147 in the following). Around the two catalytic cysteines, two conserved motifs were found that also occur in aspartate racemase: AlaCysAsnThrAla, residues 69−72, and GlyCysThrHis, residues 177−180 (Cys73/Cys184 of *L. fermentii* MurI correspond to Cys70/Cys178 in *A. pyrophilus* MurI, *10*). The bound inhibitor D-glutamine is complexed by the two cysteines, and the low RMSD of 0.72 Å between the inhibitor bound and ligand-free crystal structures indicates that the enzyme does not undergo a major conformational change upon binding. However, instead of the Cα undergoing racemization it is the C*δ* of the amide group that is ligated, a feature that is difficult to integrate into the concept of the two base mechanism (*5*, *7*). It is important to mention that *A. pyrophilus* MurI is a modestly thermophilic and not very efficient enzyme. Its k_{cat} increases by a factor of only four between room temperature and 358 K, the temperature optimum, and the k_{cat} of *L. fermentii* MurI is 100-fold higher (*1*, *12*). However, the high sequence similarity and overall arrangement suggest similar mechanisms for *A. pyrophilius* and *L. fermentii* MurI.

On the basis of the crystal structure of *A. pyrophilus* MurI, the present molecular dynamics (MD) study aims to explore fundamental aspects of the mechanism of glutamate racemase that have not yet been answered experimentally or are not accessible to experiment. What is the functional protonation state of the substrate and the active site? What are the principal residues involved in substrate binding and positioning of the catalytic cysteines? Are there different binding modes for the binding of each enantiomer? Do the two protonation states of the active site cysteines favor the binding of only one enantiomer in a catalytically competent conformation, i.e., is the stereospecifity of deprotonation the same as in *L. fermentii* MurI? This paper explores prerequisites for efficient catalysis in glutamate racemase and demonstrates that classical MD simulation is a powerful tool in exploring these ground-state phenomena.

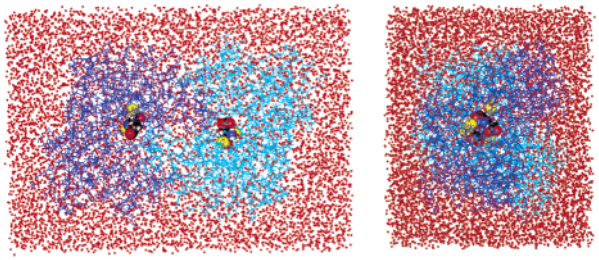

FIGURE 1: Orthogonal views of the MurI dimer (α in light blue, *β* in dark blue) immersed in an orthogonal 55 × 63 × 90 Å TIP3 water box. TIP3 waters are shown as small red spheres, D/L-Glu as well as the sulfur atoms of the catalytic cysteines are shown as CPK models (carbon is shown in black, hydrogen is in white, oxygen is in red, nitrogen is in blue, and sulfur is in yellow). The systems consisted of approximately 32 000 atoms.

METHODS

MD Setup. The starting coordinates of the glutamate racemase homodimer were taken from the X-ray structure of the enzyme complexed with the inhibitor D-glutamine, which was solved at 2.3 Å resolution (PDB entry 1B74, *11*). After deletion of the inhibitor coordinates, the substrates D-glutamate and L-glutamate were modeled into one of the two active sites. The protonation state of the cysteine proximal to the Hα was chosen as deprotonated. A total of seven different systems were set up to explore various aspects of the mechanism; the systems are abbreviated by three capital letters. Table 1 summarizes the differences in the preparation of initial coordinates and the constraints imposed during minimization and dynamics. The academic version of program CHARMM and CHARMM27 parameters (version c27b4, *13*) was used for all MD simulations. Initial coordinates were prepared by the following procedure: (i) building of hydrogen atoms and minimization of the substrate (unless mentioned, Asp, Glu, Lys, and Arg residues were ionized), (ii) alignment with an equilibrated TIP3P orthogonal water box (55 × 63 × 90 Å) and deletion of solvent molecules overlapping with the protein (2.8 Å cutoff), and (iii) minimization of solvent molecules, followed by minimization of the entire system. Figure 1 shows the MurI dimer in the TIP3 water box. Before dynamics, the system was heated stepwise to 358 K over 180 ps. Initial restraints, if any, were taken off after 240 ps and a total of up to 2100 ps periodic boundary MD simulation were performed. Through-

out equilibration and dynamics, the cutoff for nonbonded interactions was 10.0 Å (for further computational details, see Supporting Information). At 358 K (but not at 298 K), some of the surface lysines and arginines showed very flexible behavior in trial MD simulations and a total of eight residues (Arg241 and lysine residues 44, 83, 108, 158, 165, 213, and 235) had to be constrained in their side chains throughout the entire simulations to achieve stable periodic boundary conditions. However, these surface residues were between 18 and 28 Å away from the active site (measured as the distance between the Cα of the substrate and the respective residue).

Individual Setups. In two initial setups, AD3 and AL2 (Table 1), each enantiomer was poised for proton abstraction by either Cys70 thiolate or Cys178 thiolate so that all stereochemical combinations were covered (details see results). To sample as much conformational space as possible, no restraints were imposed in these two setups. All further simulations started from the same initial coordinate set as AL2 (apart from protonation in HIS and GLU), but a restraint was imposed on both S···Hα distances during minimization and equilibration (Table 1).

MD Analysis. Equilibration was verified by monitoring the RMSD of protein backbone heavy atoms. All systems equilibrated within 300 ps (see Supporting Information, Figure 1). In some of the systems, a transition in the substrate binding mode occurred during the dynamics. In this case, the individual frames were monitored to identify homogeneous parts of the trajectories. Only homogeneous and equilibrated parts of the trajectory were used for further analysis and reporting of average structures. Unless a time window is given, average values refer to the whole trajectory after equilibration. Visualization of the analysis results was carried out using the programs Pymol (*14*), MIDAS (*15*), and gOpenMol (*16*).

RESULTS AND DISCUSSION

Definition of Near-Attack Conformers in MurI. Near-attack conformers (NACs) present a region of conformation space that every molecule *has* to pass to undergo reaction (*17*); therefore, the fraction of sampled conformers present as NACs gives a measure of the likelihood of a given system to undergo reaction. In the present paper, we use the NAC concept to identify catalytically competent systems among the several setups. In previous works, NACs were defined as having a distance of less than the combined van der Waals radii of the atoms forming a new bond and an attack angle deviating by ~15° from the transition state (*18*). However, this work is the first to explore the NAC concept in terms of a trimolecular reaction (although rendered unimolecular in the enzyme substrate complex) and the Cα−thiol hydrogen distance comes in as a additional parameter. The reaction catalyzed by MurI is quasi-trimolecular because deprotonation of the substrate is not sufficient to achieve racemization: the enzyme needs to abstract the Glu Hα with its thiolate base and donate a proton to the enolate Cα from the opposite site with its thiol acid to achieve racemization. Because protonation of the enolate intermediate is likely to be instantaneous (Scheme 1), the proton donating cysteine thiol is required to be as close as possible to the forming enolate−Cα to favor racemization rather than retention.

Scheme 2: Definition of MurI Near Attack Conformers (NACs) as Conformers that Simultaneously Have a d(S···Hα) below 3.5 Å and a d(SH···Cα) below 4.0 Å

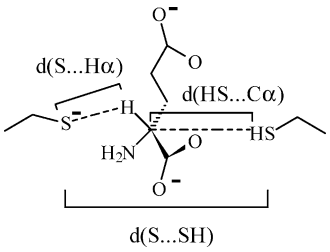

NACs are therefore defined as simultaneously having an S···Hα distance below 3.5 Å and an SH···Cα distance below 4.0 Å (vdW radii plus angle tolerance). The SH···S distance of 8.0 ± 1.2 Å presents an intrinsic geometric constraint on the angles encountered in these NACs that are (110 ± 13)° and (139 ± 18)° for the attack angles Cβ-S−Hα and S−Hα-Cα, respectively (D-Glu in the AL3). This NAC definition integrates the requirements of the two partial reactions that constitute racemization, regardless of whether the mechanism turns out to be stepwise or concerted.

Stereospecifity of Deprotonation. Biochemical studies on *L. fermentii* MurI showed that each of the thiols is exclusively responsible for the deprotonation of one of the enantiomers (*8*). To test whether this also applies to *A. pyrophilus* MurI (and whether MD simulations can capture this feature), we performed two sets of unrestrained MD simulations in which D-Glu was poised for deprotonation by the thiolates of Cys70 (AL2) and Cys178 (AD3) and vice versa for L-Glu in the other subunit. The available crystal structure of MurI with the bound inhibitor D-Gln cannot be used as a starting structure for MD simulations because it represents an unreactive binding state (*11*). We argue below that this is due to the different protonation state of the substrate under the crystallization conditions. Instead, the coordinates of D-Gln were deleted and a pair of Glu enantiomers was modeled into the two active sites. Docking was guided by the idea that a minimal displacement in the positions of Cα and α-amino group should occur during racemization, in a manner that reflects the symmetrical arrangement of the active site (Figure 2A); a similar ligation was suggested for aspartate racemase (*2*).

The catalytic cysteine residues are part of the conserved AAR-signature motifs AlaCysAsnThrAla (residues 69−72) and GlyCysThrHis (residues 177−180); each cysteine is

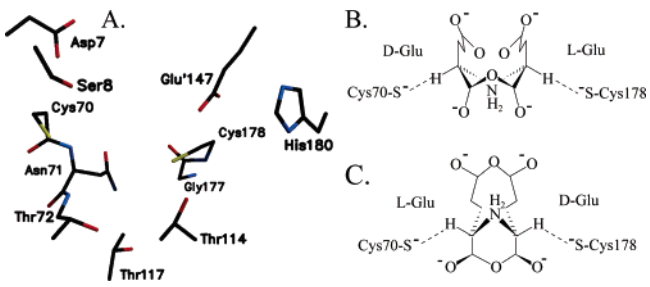

FIGURE 2: (A) Crystal structure of the active site (PDB entry 1B74; same color code as in Figure 1). The bound inhibitor D-Gln was deleted to allow docking of a pair of Glu enantiomers according to panels B and C to the right. Overlay of the modeled Glu enantiomers in the starting structures of AL2 (B) and AD3 (C) shown in the same orientation as in panel A. AL2 and AD3 cover all possible stereochemical combinations.

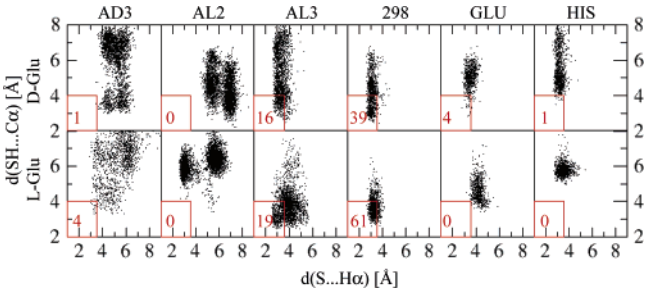

FIGURE 3: Distribution of conformers along the S···Hα vs SH···Cα distances (Scheme 2). The NAC region is marked as red box. The molfraction in % of NACs in equilibrated trajectories (typically 0.3−2.1 ns) is given as a red number in the NAC region; the upper panels pertain to D-Glu, the lower panels pertain to L-Glu. Assignment of stereochemistry of deprotonation is based on setups AD3 and AL2 (for details on setups, see Table 1). In AD3, conformers move away from the NAC region. In both enantiomers of AL2, conformers fulfill only one of the distance requirements. Application of initial restraints in AL3 resolves this flaw of AL2. Comparison of AL3 and 298 simulation (run at 358 and 298 K, respectively) shows that NAC formation competes with thermal motion; the fluctuation in the AL3 trajectory is due to weak ligation of the substrate. Protonation of the Glu α-amino group (GLU) or the imidazole group of His180 (HIS) introduces stabilizing interactions that lock the substrate in conformations unfavorable for NAC formation. This suggests that the catalytically competent protonation state is that of AL3.

flanked by two hydrogen bond donors, Ser8/Asn71 and His180/Gly177, and an acidic residue, Asp7 and Glu′147. If the substrate is docked so that its Cα is between the two cysteines, its two carboxylates can point either into a flexible pocket formed by the conserved threonine residues 72, 114, and 117 (referred to as "threonine pocket" in the following) or into the void between the carboxylates of Asp7 and Glu′147. The α-carboxylate was placed into the threonine pocket and the *δ*-carboxylate was placed between the two carboxylate side chains of Asp7 and Glu′147 so that the Glu Cα was sandwiched between the catalytic thiols (Figures 2B and 2C). In AL2, this arrangement resulted in a close contact of the D/L-Glu α-amino group and the amide groups of Asn71, whereas in AD3, the Glu α-amino group pointed into the void between the Asp7 and Glu′147 carboxylates, without any close contact to an active site residue.

AL2 developed stable binding patterns in which both enantiomers made several stable hydrogen bonds to active site residues through their α-carboxylate and α-amino groups while maintaining Cα in close contact to Cys70 and Cys178. In AD3, ligation was restricted to a stacking of the Glu carboxylates to the Thr72/Asn71 amides. Eventually, the missing contacts between the α-amino group and the Asn71 amide groups proved to be critical and the poor ligation resulted in a dissociation of D-Glu from the active site in the later stage of the AD3 simulation, accompanied by an opening of the active site channel (vide infra). Although both simulations have poor NAC yields (Figure 3), we argue that AL2 rather than AD3 represents the catalytically relevant stereochemistry. There are two obvious flaws in AL2 that account for the absence of NACs: (i) in the D-Glu ligating subunit, a transition occurs during heating up into what we describe below as a "flipped" binding state (Figure 7A); (ii) in the L-Glu ligating subunit, Cys70 thiol faces away from the active site by almost 180° (Figure 7B). This is illustrated by Figure 3: In both enantiomers of AL2, there are binding states that meet only one of the NAC distance criteria, whereas the distribution of conformers in AD3 is almost completely disperse and the small number of NACs is a remainder of the starting coordinates. The application of constraints during equilibration (AL3) relieved the flaws present in AL2 and, while maintaining similar binding patterns, resulted in high NAC yields (Figure 3). This suggests that Cys70 and Cys178 deprotonate D-Glu and L-Glu, respectively, in analogy to the stereospecifity observed in *L. fermentii* MurI. We therefore consider AL3 to represent the catalytically competent system and draw our conclusions on substrate ligation and thiol/thiolate positioning exclusively from AL3 and, to a minor extent, AL2 and 298.

Substrate and Active Site Protonation State. Several studies on MurI and proline racemase have shown that the protonation state of the active site is of crucial importance to catalysis (*6*, *8*). Apart from the catalytic cysteines, there are only two side chain groups of active site residues whose standard pK_a values fall into the range of the pH optimum *of A. pyrophilus* MurI, pH 8.5 (*12*): the imidazole moiety of His180 and the α-amino group of the substrate. In this respect, it is important to consider that aliphatic amino groups and imidazoles have large heats of ionization, i.e., their pK_a decreases significantly at higher temperatures (*19*). Using a ΔH_I° value of 13 kcal mol^{-1} and van't Hoff's equation, a calculation for the α-amino group of Glu yields a pK_a of 8.0 at 358 K as opposed to a value of 9.6 at room temperature (see Supporting Information, *19*). At pH 8.5, 76% of Glu in solution is deprotonated, and we therefore also chose the α-amino group of the bound substrate to be deprotonated. Under the crystallization conditions (pH 6.5, 18 °C), however, the α-amino group of the inhibitor D-glutamine is quantitatively protonated in solution (99.92%), and the substrate is likely to be bound in this state. Because of the strong ionic interaction of its ammonium group with the side chain carboxylates of Asp7 and Glu′147, protonation of the substrate could lead to an inverted ligation in which the *δ*-carbon instead of the α-carbon is placed between the two catalytic cysteines (*11*). Although the pK_a shifts are in accord with D/L-Glu and His180 being deprotonated at high temperature, it is impossible to extrapolate solution to active site pK_a. For this reason, we have carried out MD simulations to test the influence of different protonation states.

A trial simulation (GLU, Table 1) in which D/L-Glu had an ammonium group instead of an amino group yielded no NACs for L-Glu and only a small percentage of NACs for D-Glu observed exclusively in the first 500 ps (Figure 3). Also, it was observed that both thiolates were continuously ligated in hydrogen bond distance by an ammonium hydrogen of the enantiomers. In view of the significantly lower pK_a of the ammonium group as compared to Hα, the thiolate is more likely to abstract a proton from the ammonium group than from Hα. This implicates that the protonated substrate could represent an inhibitor that converts the enzyme into a noncatalytic protonation state.

In a system in which His180 was protonated (HIS, Table 1), the absence of NACs for L-Glu (Figure 3) is due to a salt bridge between the imidazolinium moiety and the α-carboxylate of L-Glu, which positions the Cα away from the Cys70 thiolate. This rules out His180 protonation to play a role in the L → D reaction, and the low fraction of NACs makes any involvement in the D → L reaction unlikely. By

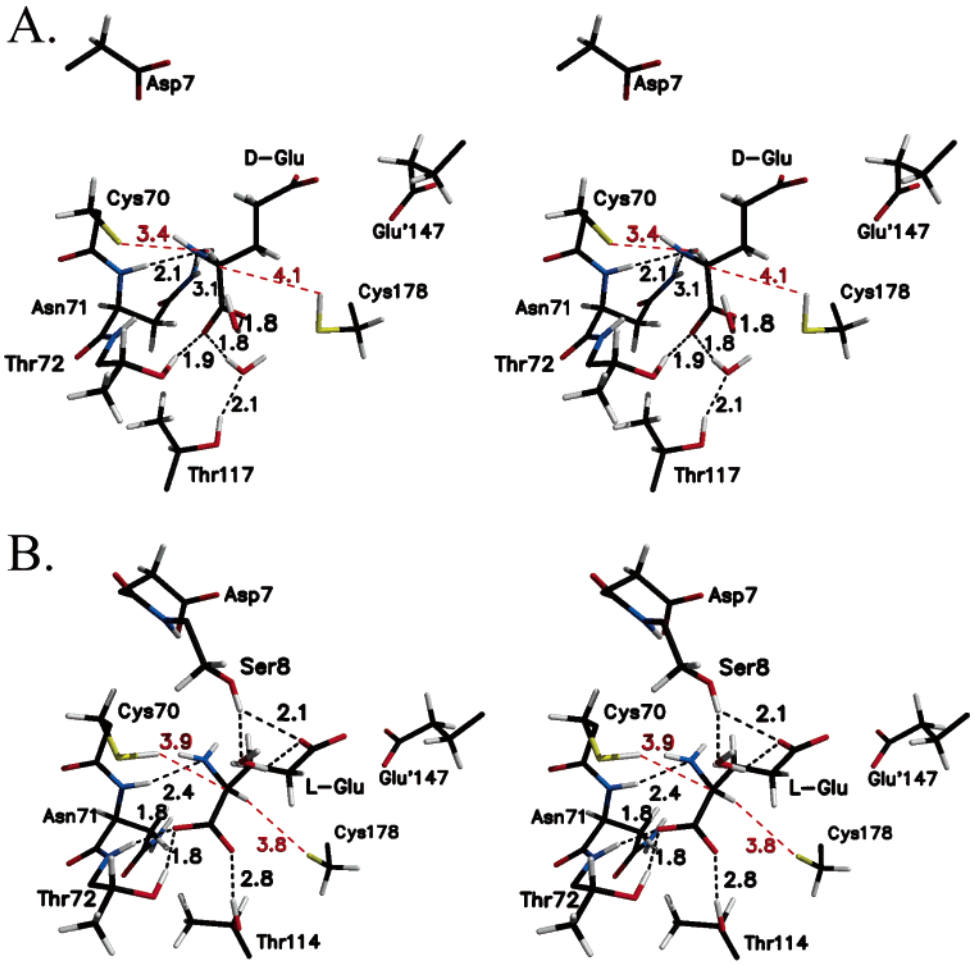

FIGURE 4: Stereoviews of the active sites binding D-Glu (A, 0.3−1.32 ns) and L-Glu (B, 0.3−1.2 ns) in AL3 (same atom color code as in Figure 2). Persistent and temporary hydrogen bonds are marked by dotted lines with their average distances (in A, the D-Glu α-N to Asn71 side chain amide distance is between heavy atoms). The two NAC defining distances are marked in red. Apart from the two cysteines, only crystal waters and residues partaking in substrate ligation are shown. Note the positioning of the Glu δ-carboxylate between the Asp7 and Glu′147 side chain carboxylates.

extension, this also excludes "activation" of the protonated substrate by proton transfer to His180 in the active site.

Considering the charge repulsion between the Glu δ-carboxylate and the two neighboring side chain carboxylates of Asp7 and Glu′147, it is conceivable that the former group displays a strongly shifted pK_a value that might enable a (partial) protonation at pH optimum, as observed, e.g., for β-galactosidase (*20*). Such a protonation can be expected to have little impact on the hydrogen bonding network between the three carboxylates and surrounding crystal waters (vide infra), nor is it expected to have an impact on the reaction chemistry.

Because the active site is highly negatively charged (a total of four ionized carboxylates plus one thiolate), the positive charges introduced by protonation in GLU and HIS lead to new salt interactions that lock the substrate in a conformation that is less favorable for racemization (Figure 3). In contrast, the trajectories of AL3 are characterized by strong fluctuations; five additional simulations that started from variations of the AL3 setup and amounted to 4 ns showed a similar behavior. As will be discussed below (cysteine positioning), this suggests that the fluctuation in the S···Hα and SH···Cα distances observed in AL3 (Figure 3) is a reproducible property of the catalytically competent system and might be involved in making the NAC region more accessible at high temperature. We therefore consider AL3 to represent the catalytically relevant protonation state and in the following results refer exclusively to this protonation state (AD3, AL2, AL3, 298).

Substrate Ligation. The active site of MurI displays a pseudo-symmetric arrangement in which each thiol halfsite is flanked by a hydrogen donor (Ser8, His180) and a negatively charged residue (Asp7, Glu′147), while Asn71 and the threonine pocket (residues 72, 114, and 117) partake in interactions with both halfsites (Figure 2A). Our simulations AL2, AL3, and 298 show that the threonine pocket, in concert with the backbone amide of Thr72 and crystal waters, provides a very flexible arrangement for accommodating the α-carboxylate group.

The threonine residues display high flexibility, and various arrangements were encountered in which two or three persistent hydrogen bonds were formed between Thr72 backbone amide, threonine hydroxyl groups, and/or crystal water and the α-carboxylate oxygens of D/L-Glu (Figure 4). The threonines that do not ligate the substrate engage in mutual hydrogen bonds between their backbone amides and hydroxyl groups (not shown).

The α-amino group of both Glu enantiomers can engage in hydrogen bonds with the backbone and side chain amide of Asn71. The hydrogen bond to the Asn71 backbone amide

is present in all simulations, except in AD3 and GLU, and functions as a hinge that persists even as the substrate changes from one binding state to another and probably also during racemization (Figures 4, 6, and 7). The Asn71 side chain amide can serve both as hydrogen bond donor and acceptor. Disruption of this interaction is critical in controlling the dissociation of the substrate from the active site (vide infra).

The substrate δ-carboxylate group hardly engages in binding interactions with active site residues and instead is steered into its position by electrostatic repulsion from the two side chain carboxylates of Asp7 and Glu147; two or three crystal waters are present in this part of the active site and form a very flexible hydrogen bond network that bridges the three carboxylates.

The significantly enantioselective effects on k_{cat} observed in mutant studies of Asp7Ser and Glu147Asn were interpreted in terms of these residues being involved in proton transfer (*11*). Our simulations rather suggest that these mutations interfere with substrate positioning by turning a repulsive carboxylate−carboxylate interaction into a possible hydrogen bond (*11*). The δ-carboxylate of D/L-Glu is situated between the Asp7 and Glu′147 carboxylates in an asymmetric fashion: e.g., the δ-carboxylate of D-Glu points toward Glu′147 and during AL3 the closest carboxylate oxygen−oxygen distance is 4.0 ± 0.2 Å (compared to 6.2 ± 1.0 Å toward Asp7), close enough to accommodate a positive interaction with Asn′147 in the Glu147Asn mutant. Likewise, the δ-carboxylate of L-Glu is situated closer to Asp7 and should be less perturbed in the mutant (again, the closest average distances between carboxylate oxygens differ by ~2.0 Å). We therefore argue that the enantioselectivity of the Asp7Ser and Glu147Asn mutants is mainly due to the role in substrate positioning of Glu′147 and Asp7: the positive interaction between the substrate δ-carboxylate and the proximal Ser7/Asn′147 residue interferes with the large displacement of the ethylcarboxylate group of Glu that is necessary for racemization (Figure 9). If this proposal holds, the mutants should display both a significantly decreased rate of deprotonation (due to the higher fraction of nonproductive protonation and reprotonation) and the protonation of the enolate intermediate might become partially rate-limiting. Although the effects might be complicated by the involvement of the Asp7 and Glu′147 loops in substrate dissociation (vide infra), kinetic isotope studies on Asp7Ser and Glu147Asn mutants would offer a way to test this proposal experimentally.

Cysteine Positioning. For racemization to occur, it is crucial that the catalytic thiolate and thiol be positioned simultaneously in maximal proximity of Hα and Cα, respectively. Restriction of the conformation space accessible to both thiols is therefore a strict prerequisite for catalysis. For a given substrate binding state, the thiol dihedral angles χ_S and χ_{SH} of Cys70 (defined in Figure 5D) remained confined to a narrow range (Figure 5B), while χ_S of Cys178 underwent several transitions and its χ_{SH} was subject to large fluctuations. We performed five additional simulations with variations of the AL3 setup (amounting to 4 ns) but observed the same freedom of motion; it seems therefore that the flexibility of Cys178 is indeed a relevant feature of MurI catalysis. Comparison of NAC formation in AL3 and 298 (Figure 3), which start from identical structures, shows that

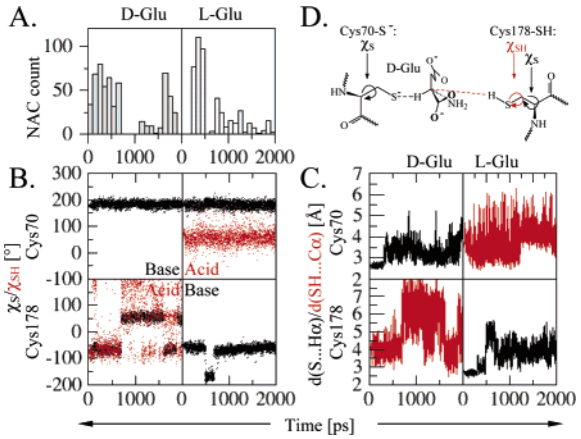

FIGURE 5: Cysteine positioning and correlation between NAC counts (A), cysteine dihedral angles χ_S and χ_{SH} (B, definition in D), and S···Hα and SH···Cα distances (C) during the AL3 dynamics (all trajectories shown from 0 to 2 ns; the left panels pertain to D-Glu, the right panels to L-Glu). The positioning of the thiol hydrogen (χ_{SH}, shown in red in B) is more flexible than that of the thiolate sulfur (χ_S, B) and the χ_S of Cys178 is more floppy than that of Cys70. This causes several transitions. Changes in χ_S and χ_{SH} affect the distance to Glu Hα and Cα, respectively, which in turn translates directly into a change in NAC yields. Note the transitions of the χ_S of Cys178 (B, lower panels) and the corresponding distances (C, lower panels) in the D-Glu trajectories at 0.7, 1.6, and 1.9 ns and in the L-Glu trajectories at 0.5, 0.7, and 1.2 ns. For example, as the transition in χ_S of Cys178 (B, lower left panel) occurs after 0.7 ns, the SH···Cα distance also increases (C, lower left panel) and the NAC count drops dramatically (A, left panel).

the frequent transitions during the AL3 dynamics can be ascribed largely to the increase in motion at the higher temperature and the weak binding of the substrate; this causes increased fluctuations in χ_S and χ_{SH}. Obviously, variations in the S···Hα/SH···Cα distances and χ_S/χ_{SH} are correlated, and this translates directly into the number of NACs formed (Figure 5).

How does the enzyme achieve conformational control in these dihedral angles and distances? This problem seems especially intriguing when one considers that the enzyme has to achieve this control for both cysteines *and* both protonation states, Cys70-S$^-$/Cys178-SH and Cys70-SH/Cys178-S$^-$.

When Cys70-S$^-$ is poised to deprotonate D-Glu, its position is stabilized by several hydrogen bonds with the neighboring Ser8 hydroxyl group and the amino hydrogens of D-Glu and, occasionally, Thr72 (Figure 6A). In the reverse reaction, when Cys70-SH is the proton donor, the thiol makes a stable hydrogen bond to the α-amino nitrogen of L-Glu (Figure 6C). In some of the simulations, Cys70-SH locks into a catalytically incompetent state in which it faces away from the active site and makes a contact to the amide backbone of Ser8 (Figure 6D). In AL3, an additional crystal water molecule forms a hydrogen bond network with the Ser8 hydroxyl group and the thiolate sulfur (Figure 6A).

As illustrated in Figure 5B, the positioning of Cys178 is more variable, because it does not benefit from the mutually stabilizing interaction with the α-amino group of Glu (Figure 6). Several stable modes of Cys178-S$^-$ positioning were encountered in AL2, AL3, and 298 (Figure 6B−D). In AL2, the side chain amide of Asn71, the backbone amide of Thr114, and a crystal water held in position by the backbone

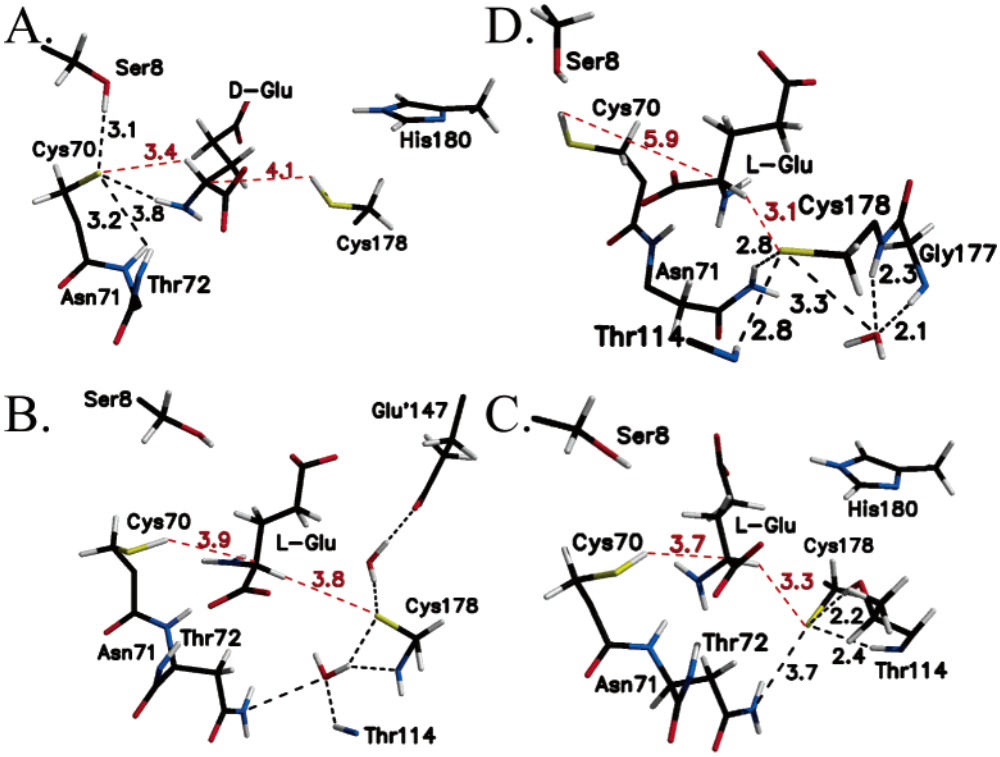

FIGURE 6: Positioning of Cys70 and Cys178 in AL3 (A, 0.3−0.7 ns; B, 0.3−1.2 ns), 298 (C, 0.3−1.3 ns) and AL2 (D, 0.24−1.08 ns). For clarity, only residues and crystal waters involved in cysteine positioning are shown (same atom color code as in Figure 1). Hydrogen bonds involved in cysteine ligation are shown as black dotted lines with their average distances; S···Hα, SH···Cα distances are marked in red. The crystal waters in panel B showed very large fluctuations; therefore, no average distances are reported. While Cys70 ligation is very reproducible (Figure 5, note similar χ_S in A−C, Figure 7A), several different patterns were found in positioning of Cys178-S$^-$ (B−D).

amides of Gly177 and Cys178 make hydrogen bonds to the thiolate and poise it for deprotonation of L-Glu (Figure 6D). In AL3, the Asn71 side chain amide is not hydrogen bonded to Cys178-SH but instead replaces the Gly177 backbone amides in positioning a crystal water; another crystal water is held in place by Glu′147 (Figure 6B). In 298, both the hydroxyl and backbone amide groups of Thr114 interact with C178-S$^-$, but crystal waters do not participate in positioning; occasionally, the side chain amide of Asn71 comes within hydrogen bonding distance of C178-S$^-$ (Figure 6C). When Cys178-SH is in position to protonate D-Glu, none of these interactions are observed and, instead, the imidazole ring of His180 moves closer and restricts the space available for rotation of the S−H bond (Figure 6A), as witnessed by the lower fluctuation of χ_{SH}(Cys178) in the first 0.7 ns of the AL3 trajectory (Figure 5B). However, the enzyme has to pay a tradeoff by occasional hydrogen bonds between Cys178-SH and the imidazole moiety of His180, which causes sharp drops in the fraction of NACs (AL3, D-Glu, 0.7−1.6 ns; Figure 5A).

Substrate Flipping. In the course of the AL2 simulation, both substrates underwent a sudden transition of their binding mode in which the substrate flipped along the axis of its carbon backbone so that the S···Hα distance increased by almost 3 Å within less than 10 ps (Figure 7). In what we term the "flipped" binding state, Glu is bound as if it was the racemization product of the opposite enantiomer: e.g., D-Glu is bound as if L-Glu had been deprotonated and received its Hα from Cys178, the proton donor in the L → D reaction (of course, no reactions can occur in MD simulations, and for this reason, the thiols have not changed their protonation state). We suggest that substrate flipping represents a propensity of the enzyme to undergo a fast response in its binding mode as racemization occurs (Figure 7C). What we observe in our MD simulations is the transition in the binding mode during racemization without the accompanying proton transfer.

In AL2 binding L-Glu, this transition is preceded by rotation of the Asn71 side chain dihedral angles that moves the side chain amide away from the substrate toward the threonine pocket (idem for D-Glu). L-Glu then ligates more tightly to the Cys70 motif and the forming hydrogen bond to Ser8 makes the substrate rotate along its principal axis. The Asn71 side chain amide develops a hydrogen bond to the Thr117 hydroxyl oxygen, and the δ-carboxylate of L-Glu forces the carboxylate of Glu′147 to form a hydrogen bond to the His180 imidazole moiety (not shown). The latter two events are the first steps in the opening of the active site (vide infra, Figure 8B).

The implication of this binding distinction is that the flipped, post-racemization state is poised for dissociation from the active site, a process that occurs on the time-scale of our MD simulations (i.e., diffusion controlled). Substrate flipping seems to trigger a mechanism by which the enzyme readily expels the substrate after racemization (vide infra). For the reverse process, substrate binding, the principle of microscopic reversibility would then predict that this mechanism ensures that active site closing leads to reverse flipping into reactive conformers.

Substrate Dissociation and Active Site Opening. Within the course of the AD3 simulation, the poor ligation of L-Glu led to an opening of the active site and a concomitant dissociation of the substrate. Initially, the active site wraps around the substrate and forms a closed cavity that only

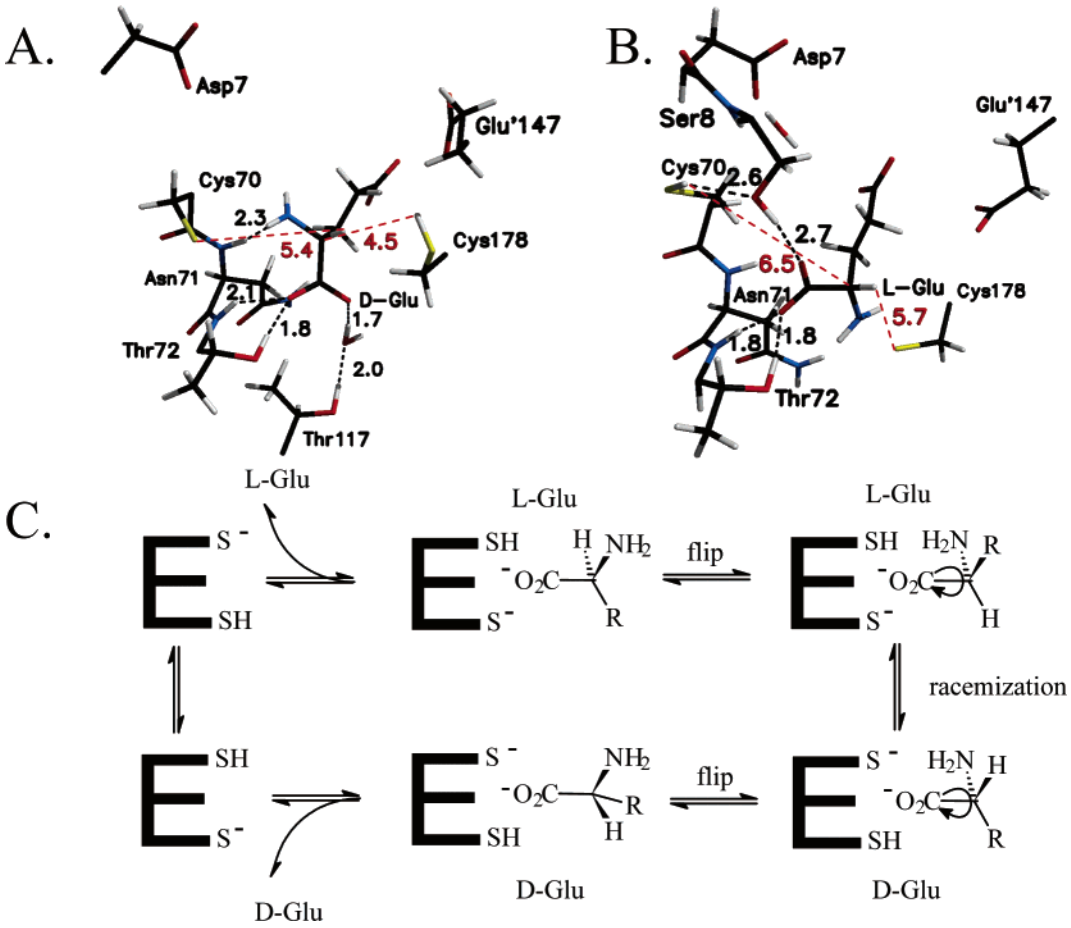

FIGURE 7: Average structures for the flipped binding states of D-Glu (A, 0.24−1.08 ns) and L-Glu (B, 1.2−2.1 ns) in AL2. In panel A, note that Hα is now closer to the thiol than the thiolate; the same would be the case in panel B, if Cys70 was in its regular position. Persistent hydrogen bonds are shown by dashed lines with their average distances; NAC distances are shown in red. (C) Extension of Scheme 1 incorporating substrate flipping as a part of the catalytic cycle. This scheme is a minimal representation and does not include the multitude of nonproductive binding states, nor the detailed steps of racemization (under physiological conditions, the cycle runs clockwise).

contains the substrate plus five to eight crystal waters (Figure 8A). The residues that surround this cavity are highly conserved across several MurI sequences (*10*). The AspSerGlyAlaGlyGly motif (residues 7−12) and the PheAlaProLeuAlaGlu motif (residues 142−147) form two loops that close the active site off from solvent access (termed Asp7 loop and Glu′147 loop in the following), together with the Asn71 side chain and the Gly177−Cys178 backbone (Figure 8). Another conserved motif, AspThrAlaArgValProProTyr (residues 33−39, conserved residues underlined), forms an unusual, eight-shaped structure in which Asp33, Arg36, and Tyr39 engage in a persistent hydrogen bond/salt bridge (not shown). This structure could provide a folding scaffold for the flexible Asp7 loop; mutation of Asp33 has drastic effects on binding (*10*).

During its dissociation from the active site, L-Glu slides along the Asn71 side chain, the α-carboxylate gradually making fewer binding contacts to the Asn71 amide groups. Meanwhile, the δ-carboxylate forces the active site to open by repulsing the carboxylates of Asp7 and Glu′147; while it maintains its distance to the Glu′147 carboxylate, it is mainly the flexible Asp7 loop in whose center the Asp7 carboxylate is situated that moves away from the δ-carboxylate. As Glu is losing all contacts to active site residues and is passing the Asp7 and Glu′147 carboxylates, the active site channel opens fully and Glu can diffuse into the solvent (Figure 8C).

Even within the short time period of our simulation, the flipped state of D-Glu encountered a similar fate. After staying in the flipped state for about 1 ns, another transition occurred in which the substrate loses contact to the threonine pocket and is only retained in the active site by two crystal waters and Asn71 backbone amide which replace the threonine pocket in ligating the α-carboxylate. In this intermediate state of substrate dissociation, the δ-carboxylate group of the substrate already sticks out of the active site pocket and becomes solvent exposed (Figure 8B). These reproducible events suggest that opening of the active site depends on the combined displacement of the Asp7 and Glu′147 loops upon the initiating movement of the Asn71 side chain toward the threonine pocket. During the active site opening, both loops undergo a transition from a compact to a stretched conformation (Figure 8, lower panels). Electrostatic repulsion between the detaching δ-carboxylate and the carboxylates of the two loops (Asp7, Glu′147) could provide the initial force that is transmitted into an opening of the active site channel via displacement of hydrophobic active side channel residues by the Asp7 and Glu′147 loops.

CONCLUSIONS

Our results show that the active site of MurI is designed to accommodate both enantiomers of Glu in a multitude of binding states. It can distinguish the enantiomers and bind

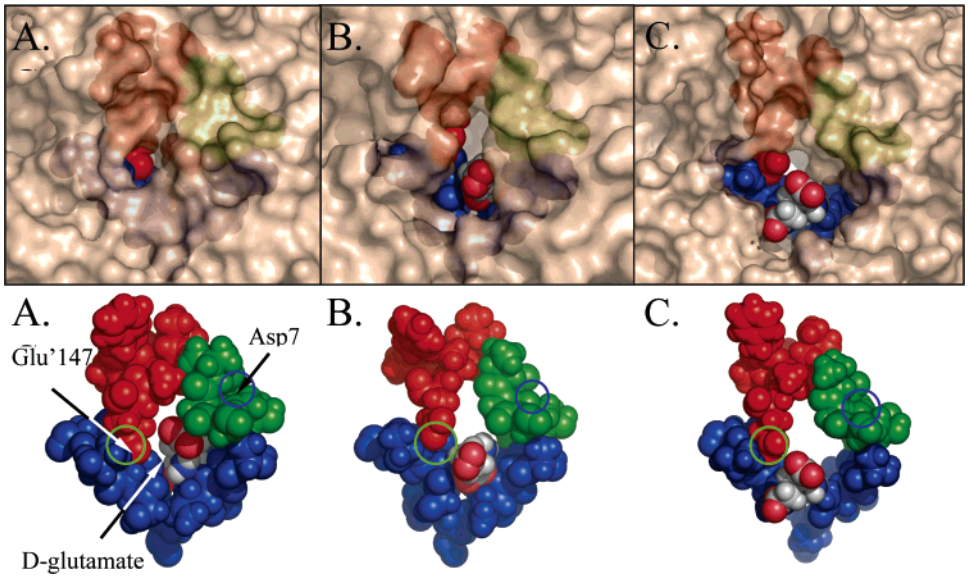

FIGURE 8: Active site opening. View of the protein surface (transparent) around the active site (upper row); the lower row shows only the active site consisting of the two cysteine motifs/threonine pocket (blue) and the Asp7 and Glu′147 loops (red and green, respectively); the substrate is shown with gray carbon, red oxygen, blue nitrogen, and white hydrogen. In the lower row, two circles indicate the position of Glu′147 and Asp7 (hidden by the loop). In the starting structure (A) and substrate binding mode, D-Glu is tightly enclosed within the active site. Panel B shows the δ-carboxylate of D-Glu protruding from the active site during an intermediate dissociative stage (AL2, 1.14−1.8 ns). Panel C shows L-Glu (AD3, 1.8 ns). Dissociation of the substrate is accompanied by gradual movement of the Asp7 and Glu′147 loops that is transmitted into an opening of the active site channel.

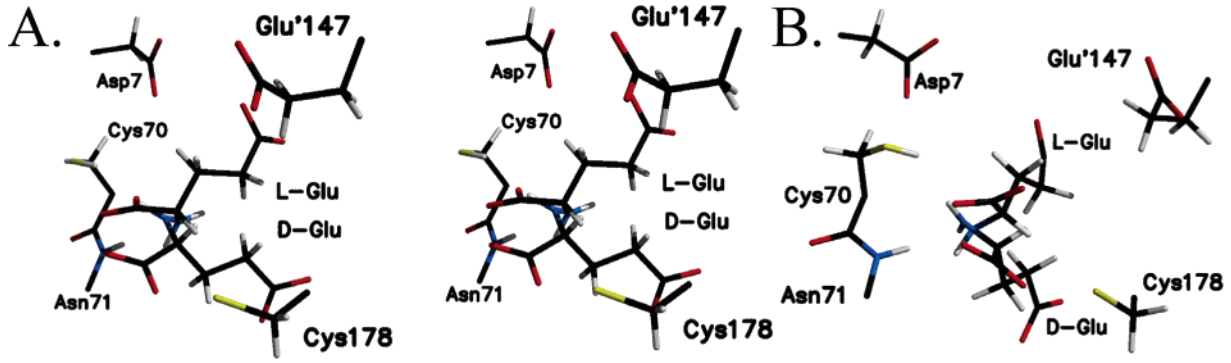

FIGURE 9: (A) Stereoview of an overlay of L-Glu bound as substrate and D-Glu in the flipped state (for clarity, only the L-Glu ligating pair of cysteines is shown). Panel B shows a rotated view of A that illustrates the pseudo-symmetry of the enantiomers. In the reaction from L- to D-Glu, the substrate is tethered to the active site via its α-amino group (ligated by the backbone amide of Asn71) and the main motion is the substrates' ethylcarboxylate moiety swinging through the empty space between the Asp7 and Glu′147 carboxylates. Note how little displacement occurs in Cα, Hα, and the α-amino group of Glu (B).

them so that each enantiomer is poised for stereospecific deprotonation exclusively by one of the two active site thiols. It can also distinguish whether a substrate has reacted or not and bind each enantiomer both as substrate and in a flipped, pre/post-racemization state. Remarkably, the later triggers dissociation of the substrate from the active site, and the reversal of this mechanism could ensure that the active site closing induced by substrate binding translates into reactive conformers.

By probing several different setups, we were able to assign the protonation state of the active site. Our simulations suggest that only Glu in which the α-amino group is deprotonated presents the substrate for MurI, whereas Glu with a protonated α-amino group could function as an inhibitor of MurI by protonating the active site thiolate. This is an intriguing suggestion that is not accessible to experiment. Protonation of His180 has a negative effect on NAC yields (Figure 3), and the role of the neutral imidazole moiety is more likely to confine the conformational space accessible to the Cys178-SH. The numerous and similar binding patterns provide an additional explanation for the low catalytic efficiency of *A. pyrophilus* MurI (k_{cat} (L → D) = 0.8 vs 70 s^{-1} for *L. fermentii* MurI, *1*, *12*). Transition between these states is fast enough to be observable in our MD simulations and thus several orders of magnitude faster than the rate-limiting proton abstraction (10^5 s^{-1} in proline racemase, *6*). The numerous binding states, not all of which are catalytically competent, and the fast transitions between them pose a strong kinetic competition to racemization.

The remarkable binding flexibility of MurI is the result of weak or even repulsive interactions with the substrate (however, the high K_m value is not detrimental because its physiological substrate, L-Glu, is quite abundant). We argue that the weak binding interactions actually play a crucial role in catalysis by MurI. As mentioned before, protonation of the intermediate or transition state enolate is a very fast reaction that is likely to happen on a time-scale of picoseconds (*6*). Accordingly, a weak bonding of the α- and

δ-carboxylates would favor reaction by allowing for a fast transition into the racemized state of the other enantiomer as witnessed in substrate flipping (vide supra). Note that the α-amino group itself would remain fixed due to its positioning by Asn71 backbone amide (Figures 7 and 9). Especially the repulsive interaction between the δ-carboxylate and Asp7/Glu′147 carboxylates is very well suited for this purpose: comparison of the substrate bound state of, e.g., D-Glu and the flipped state of L-Glu, shows that the major displacement occurs in the ethylcarboxylate moiety (Figure 9). A repulsive interaction allows for maximal flexibility; only the flexible hydrogen bond network with the surrounding crystal waters needs to be rearranged and the relaxation into the new binding state can occur in parallel to the protonation. In a similar fashion, the highly promiscuous threonine pocket allows a sliding from one α-carboxylate binding state into another simply by rotation.

ACKNOWLEDGMENT

A part of the Gaussian98 and MD calculations were performed on the IBM p690 cluster at University of Illinois at Urbana-Champaign (NCSA). H.M. thanks Swarnalatha Reddy for helpful discussions and continuous support.

SUPPORTING INFORMATION AVAILABLE

Contains additional details of MD methods and calculation of pK_a(358 K) of Glu α-amino group and a copy of ref *19*. This material is available free of charge via the Internet at http://pubs.acs.org.

REFERENCES

1. Gallo, K. A., and Knowles, J. R.(1993) Purification, cloning, and cofactor independence of glutamate racemase from Lactobacillus, *Biochemistry 32*, 3981−3990.
2. Liu, L., Iwata, K., Kita, A., Kawarabayasi, Y., Yohda, M., and Miki, K. (2002) Crystal structure of aspartate racemase from *Pyrococcus horikoshii OT3* and its implications for molecular mechanism of PLP-independent racemization, *J. Mol. Biol. 319*, 479−489.
3. Koo, C. W., and Blanchard, J. S. (1999) Chemical mechanism of *Haemophilus influenzae* Diaminopimelate racemase, *Biochemistry 38*, 4416−4422.
4. Cardinale, G. J., and Abeles, R. H. (1968) Purification and mechanism of action of proline racemase, *Biochemistry 7*, 3970−3978.
5. Rudnick, G., and Abeles, R. H. (1975) Reaction mechanism and structure of the active site of proline racemase, *Biochemistry 14*, 4515−4522.
6. Albery, W. J., and Knowles, J. R. (1986) Energetics and mechanism of proline racemase, *Biochemistry 25*, 2572−2577.
7. Gallo, K. A., Tanner, M. E., and Knowles, J. R. (1993) Mechanism of the reaction catalyzed by glutamate racemase, *Biochemistry 32*, 3991−3997.
8. Tanner, M. E., Gallo, K. A., and Knowles, J. R. (1993) Isotope effects and the identification of catalytic residues in the reaction catalyzed by glutamate racemase, *Biochemistry 32*, 3998−4006.
9. Glavas, S., and Tanner, M. E. (2001) Active site residues of glutamate racemase, *Biochemistry 40*, 6199−6204.
10. Glavas, S., and Tanner, M. E. (1999) Catalytic acide/base residues of glutamate racemase, *Biochemistry 38*, 4106−4113.
11. Hwang, K. Y., Cho, C. S., Kim, S. S., Sung, H. C., Yu, Y. G., and Cho, Y (1999) Structure and mechanism of glutamate racemase from *Aquifex pyrophilus*, *Nat. Struct. Biol. 6*, 422−426.
12. Kim, S. S., Choi, I. G., Kim, S. H., and Yu, Y. G. (1999) Molecular cloning, expression, and characterization of a thermostable glutamate racemase from a hyperthermophilic bacterium, *Aquifex pyrophilus*, *Extremophiles 3*, 175−183.
13. Brooks, B. R., Bruccoleri, R. E., Olason, B. D., States, D. J., Swaminathan, S., and Karplus, M. J. (1983) CHARMM: A Program for Macromolecular Energy, Minimization, and Dynamics Calculations, *J. Comput. Chem. 4*, 187.
14. DeLano, W. L. (2003) The PyMOL molecular graphics system. Version 0−93. DeLano Scientific LLC, San Carlos, CA. http://www.pymol.org/.
15. Ferrin, T. E., Huang, C. C., Jarvis, L. E., and Langridge, R. (1988) The Midas display system. *J. Mol. Graphics 6*, 13−27.
16. Laaksonen, L. (1992) gOpenMol, a graphics program for the analysis and display of molecular dynamics trajectories. Version 2.10., Center for Scientific Computing, Espoo, Finland. http://www.csc.fi/gopenmol/.
17. Bruice, T. C. (2002) A view at the millennium: the efficiency of enzymatic catalysis, *Acc. Chem. Res. 35*, 139−148.
18. Hur, S., and Bruice, T. C. (2003) The near attack conformation approach to the study of the chorismate to prephenate reaction, *Proc. Natl. Acad. Sci. U.S.A. 100*, 12015−12020.
19. Cohn, E. J., and Edsall, J. T. (1943) Protein amino acids and pepides as ions and dipolar ions, ACS Monographs Series, pp 81−82, American Chemical Society, Washington, DC.
20. Richard, J. P., Huber, R. E., and McCall, D. A. (2001) Effect of an E461G mutation of β-galactosidase (*Escherichia coli*, lacZ) on pL rate profiles and solvent deuterium effects, *Bioorg. Chem. 29*, 146−155.

BI049580T